Evaluating Complexation of Common Metal Cations by Cyanins: Molecular Structure, Binding Affinity and Optical Properties

Laura Estévez,[a] Marta Sánchez-Lozano[a,b] and Ricardo A. Mosquera[a]

[a] Departamento de Química Física, Facultade de Química, Universidade de Vigo, Lagoas-Marcosende s/n, 36310-Vigo, Galicia, Spain.
[b] Current address: CEAMSA, R&D Department, As Gándaras, 36418-Porriño, Galicia (Spain).

lestevez@uvigo.es

ABSTRACT

The ability of anthocyanins to bind metal ions has been exploited for several purposes, including, to stabilize anthocyanins from natural sources, color control in food chemistry or as an analytic method for determination of metals concentrations by using UV–vis spectroscopy. Bearing this potential in mind, we were keen on investigating the ability of diverse metal cations to form complexes with cyanin by means of Density Functional Theory (DFT) together with time dependent (TD) DFT and the Quantum Theory of Atoms in Molecules (QTAIM). These theoretical methods have been employed to gain insights into fundamental aspects of their chemical bonding as well as on their electronic and optical properties. Our results indicate that Na^+ and K^+ give rise to the most labile complexes, whereas the strongest preference is shown by trivalent metals which exceed that of Mg(II), indicating that ion replacement processes are suitable detoxification mechanisms for plants. QTAIM analysis allow us to describe their formation as ligand to metal charge transfer (LMCT) complexes where the stronger the binding the larger the charge transfer. Upon metal complexation the cyanin ligand molecular structure is more compatible with a dienolate-like structure rather than the 4'-keto-quinoidal-like structure where the weight of the latter increases as stronger the binding with the metal ion. UV-vis spectra of most of the metal complexes studied here feature a strong band absorption in the visible region at longer wavelength than free cyanin at low pH values. Also, bathochromic wavelength shifts are observed, *e.g.*, with Fe(II) or Fe(III) that exceeds that with Al(III). After examination of their Frontier Molecular Orbitals, visible light absorption is consistent with charge transfer $\pi \rightarrow \pi^*$ electronic transition taking place mainly within the dye.

KEYWORDS

Metal anthocyanins, cyanidin, metal detoxification, metal affinity, bathochromic effect

1. Introduction

The formation of complexes between metal cations and anthocyanins was firstly proposed in 1919 by K. Shibata *et al*. [1] for explaining why cyanin, red in strongly acid media and colorless in aqueous solution within the acidic pH range of sap, provides blue color in the flowers of *Centaurea cyanum*. Since then, most of the research carried out on the structure of metal-anthocyanin complexes aimed to solve a long controversy about flower and fruit pigmentation, [2] in particular, about the mechanism to allow blue hues in mildly acidic aqueous environments. [3] Regarding this latter, an interaction between the blue quinoidal base (anion form) and other colourless organic compounds (copigments) [4] or metallic ions has been claimed as responsible for blue coloration at pH values where otherwise anthocyanins would suffer discoloration. [5,6] For metal complexation, anthocyanins, featuring a catechol moiety in the B-ring, might lose two protons to bind metal ions. [7,8] Metal complexation, therefore, would be predominant at pH 6-8 were the anionic species is the major one. [9] Alternatively, at lower pH values, metal ions could shift the anthocyanin equilibrium toward the more reactive species for metal complexation (Scheme 1). Overall, this process is controlled by the pH of the medium and the acidity of the metal ion, since this latter must compete with protons for binding sites. [10]

Nowadays, diverse practical aspects have promoted an increasing interest on metal-anthocyanin complexes. Thus, they are considered an interesting alternative to replace synthetic food colorants [11] or as textile dyes, [12] as metal complexation would allow the persistence of pigmentation at higher pH. Metal-anthocyanin complexes are expected, as well, to play an important role in metal detoxification mechanisms into the plant vacuoles, [13] where anthocyanins and metal excess are accumulated. Metal-anthocyanin chelates have also been considered responsible for skin darkened discoloration of diverse

fruits. [14] As a result, metal complexation by anthocyanins has been extensively invoked in very different fields of chemical literature. [15-18]

Scheme 1. pH dependent mechanism for Cyanidin-*3,5-O*-diglucoside-metal complexation. The two glycosyl groups attached to O3 and O5 of the aglycon skeleton (cyanidin) have been replaced by methyl groups. Main labels have been introduced. Energy difference (ΔE, in kcal·mol^{-1}) between neutral and anion tautomers of cyanin when complexed by M=Al(III).

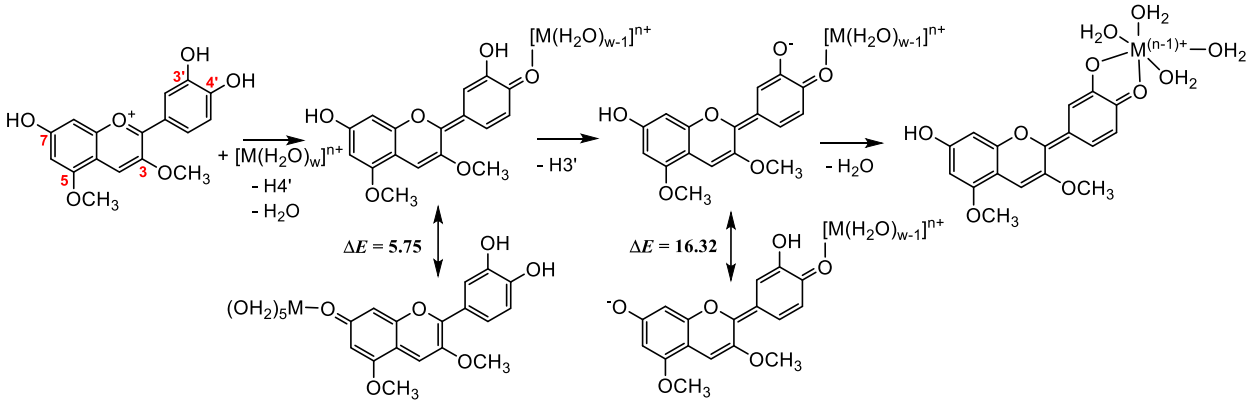

Nevertheless, despite the interest of these complexes, computational studies dedicated to anthocyanin-metal complexation are very scarce, [19-21] especially, when compared to the number of studies carried out on metal-quercetin, [22-24] or on copigment-anthocyanin. [9,25,26]

This work aims to quantify, making use of quantum chemical calculations, the stability of the complexes formed by the quinoidal base anion, which governs complexation, [5,6] of cyanidin-3,5-O-diglucoside with the most common metallic cations in natural environments. Metal cations, M^{n+}, included in this work were selected taking into account their natural abundance and/or environmental significance. Therefore, a series of 12 metal cations were included in this study; Na^+, K^+, Mg(II), Ca(II), Al(III) and first row transition metals Cr(II)/Cr(III), Mn(II), Fe(II)/Fe(III), Co(II)/Co(III), Ni(II),

Cu(II), and Zn(II). Cyanin has been selected, to explore metal-complexation with anthocyanins, because it displays the necessary dihydroxy substitution pattern on the B-ring to bind metals. Therefore, this latter together with its ubiquity in Nature make metal-cyanin complexes convenient as the target of our study.

Overall, this work seeks to shed light on the fundamental aspects of the chemical bonding in metal-anthocyanin complexes as well as investigating the role of the metal ion in the optical properties of these complexes (*e.g.*, bathochromic effect upon metal complexation). To this end we will make use of density functional theory DFT as well as Time Dependent DFT (TDDFT) calculations together with Bader's Quantum Theory of Atoms in Molecules (QTAIM), [27,28] as this methodology provides useful descriptors for characterizing the bonding.

2. Material and method

2.1. Model compounds

In order to reduce the computational cost, we have assumed negligible the effect of the glucose substituents on the metal-cyanin binding. Indeed, this has been corroborated, previously, by some of us. [20] In addition, synthetic analogues of anthocyanins, lacking O-glucose groups at C3 and C5 positions, have been shown to be a useful model system for metal-anthocyanin complexation studies, pointing to that the replacement of the glucose by a methyl group is expected not to play any role on metal complexation (as it happens with the anthocyanin chromophore). [29] Therefore, cyanin is modeled replacing the glucose groups attached to O3 and O5 by methyl ones (Scheme 1). The methyl groups are orientated so that the aglycon is in the same disposition determined for the glycosyl groups in the X-ray diffraction study of the protocyanin crystal. [30] This avoids

important steric hindrances (C2-C3-O3-CH3 in -*anti* and C6-C5-O5-CH3 in –*syn*). In previous studies it has been found that the most stable anionic form of cyanidin is obtained extracting protons from hydroxyls bonded to C5 and C4'. [31] The near isoenergetic anion **A74'** (that obtained by extracting protons of C7-OH and C4'-OH) would be the most stable in cyanidin-3,5-*O*-dimethoxide. However, this would not have to be longer true in the presence of metal ions. Indeed, we have conducted a series of calculations which indicate that metal complexation is more favored at C4' than at C7 by 5.75 kcal·mol^{-1}. After monodentate complexation at C4', H3' becomes indeed more acid (deprotonation at C3' is favored by 16.32 kcal·mol^{-1} over deprotonation at C7) due most likely to the stabilization inferred by water molecules of the hydrated metal ion and subsequent complexation at C3' would take place to reach the bidentate-like structure (Scheme 1). These theoretical results would reinforce the experimental evidences showing that metal complexation is restricted to 3',4'-dihydroxyflaviliums where anthocyanins behave as bidentate ligands. Therefore, the cyanin quinoidal base anion, hereafter Cy^-, involved in the binding with metal cations might be that resulting from deprotonation of the hydroxyl groups attached to C3' and C4'.

Cy^- optimized molecular structure is completely flat. The distance between O3' and O4' (bite distance) is 2.795 Å in PCM modeled aqueous solution. As previously observed in the neutral or anionic tautomers were one or several B-ring hydroxyls have been deprotonated, [31] the C2-C1' bond length, is significantly shorter than in the cyanidin cation (respectively, 1.406 Å and 1.443 Å, in water modeled with PCM). This has been explained in terms of resonance forms, considering significant participation of quinoidal structures for ring B (Scheme 2).

The geometries of metal hydrated ions, $[M(H_2O)_w]^{n+}$, in their diverse possible stoichiometry ratios according to chemical literature (w= 4 and/or 6), and the corresponding $[MCy(H_2O)_{w-2}]^{(n-1)+}$ complexes were obtained by means of density

functional theory, DFT, where different M^{n+}:Cy ratios could be envisioned. Nonetheless, 1:1 stoichiometry ratio has been reported to be the dominant species, [32-34] while 1:2 or 1:3 M^{n+}:anthocyanin ratios have been proposed to occur when a large excess of metal is available or at high pH values, in a similar fashion as catechol does. [35] All together, this study is concentrated on 1:1 $[MCy(H_2O)_{w-2}]^{(n-1)+}$ complexes. However, we have extended our study to 1:2 $[FeCy_2(H_2O)_{w-4}]^+$ complexes/or ***SP*-4** $[FeCy_2]^+$ and ***OC*-6** $[FeCy_2(H_2O)_2]^+$. The reason for this selection was based on experimental results that evidenced that the stoichiometry of complexes of Fe(III) ions with Cyanin could reach 1:2 ratios. [36]

Scheme 2. Main resonance forms for the model of anionic cyanin.

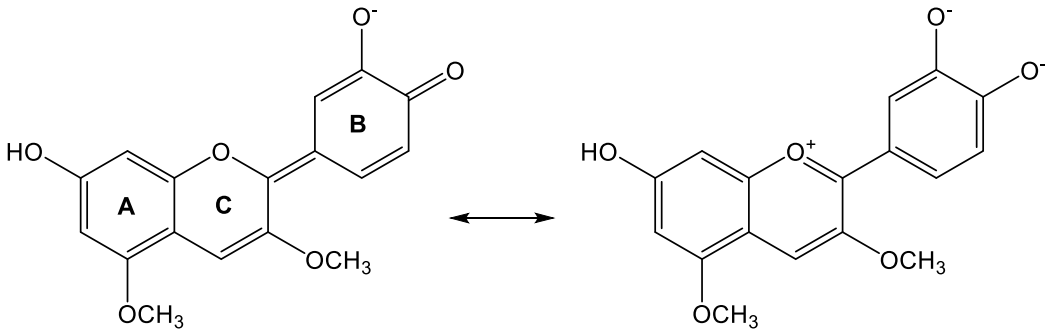

2.2. Computational details

All the model compounds were fully optimized, modeling the aqueous solvated form with the polarizable continuum model (PCM), [37] at the B3LYP/6-31++G(d,p) level using the Gaussian-09 program. [38] Thermal corrections to the energy were taken from optimizations in the gas phase, as previously done. [20] In all cases, all electrons basis sets were used for the M^{n+} cations. B3LYP [39] has been selected as this density functional and similar computational levels have been found to provide results that are in good agreement with experimental data. [22,23] In addition, to account for dispersion

effects B3LYP energies were corrected with the Grimme's D3 dispersion correction. [40] Furthermore, when necessary, basis set superposition errors (BSSE) were accounted by employing the counterpoise correction (CP) introduced by Boys and Bernardi. [41] The allowed excitations and oscillator strengths together with electronic absorption spectra of the most stable $[MCy(H_2O)_{w-2}]^{(n-1)+}$ complexes investigated in this work were obtained by single point calculations on their corresponding optimized ground state geometries by means of time-dependent (TD) method, as implemented in Gaussian09, at the TD/B3LYP/6-31++G(d,p)/PCM// B3LYP/6-31++G(d,p)/PCM) level of theory.

Ground state electron densities, $\rho(\mathbf{r})$, were analyzed within the context of the QTAIM [27,28] with AIMAll program. [42] This theory partitions molecules into disjoint atoms, Ω, given by the basins for the gradient of the electron density, $\nabla\rho(\mathbf{r})$. Each of them (with few exceptions) contains one nucleus. These atoms are connected by a set of links, known as bond paths, which usually recover the Lewis structure of the molecule. Bond paths are obtained by conducting $\nabla\rho(\mathbf{r})$ from the diverse (3,-1) singular points of $\rho(\mathbf{r})$ field. These points are named bond critical points (BCPs), and the value displayed at one of them by the electron density, ρ_b, is a relative measure for the strengths of bonds connecting the same pair of elements. The Laplacian of $\rho(\mathbf{r})$ at the BCP, $\nabla^2\rho_b$, or the corresponding value of the total energy density function, H_b, indicate the ionic (positive values) or covalent (negative ones) nature for the bond. The QTAIM atomic charge of the metal atom in the complexes, Q_M, was obtained by integrating $\rho(\mathbf{r})$ over the corresponding atomic basin. This integration yields the atomic electron population for the atom, which turns into Q_M after subtracting it from the atomic number, Z. We have mostly focused on atomic charge variation upon complex formation, ΔQ_M as well as on M-O3', M-O4' BCP properties to shed light on the origin of the Cy-M^{n+} bond and rationalize the preference of Cy^- for metallic cations.

3. Results and discussion

3.1. Optimized structures for hydrated cations

We have optimized (with no symmetry restrictions) hexaaqua and tetraaqua complexes from, respectively, pseudo initial Oh and Td geometries, for every metallic cation indicated above. The preference between these coordination numbers is evaluated through $\Delta_1 E$ (Table S1), which is defined as the CP corrected energy for process (1).

$$[M(H_2O)_6]^{n+}\,(aq) \rightarrow [M(H_2O)_4]^{n+}\,(aq) + 2\,H_2O\,(aq) \qquad (1)$$

Experimental evidences indicate that hexa-coordinated hydration is favored over tetra-coordination and our DFT results are in good agreement with this experimental trend. With no exception and in agreement with water being a weak-field ligand, the most stable aqua complexes of 3d transition metals explored here resulted to be of high spin.

As expected, in the high spin $[Cr(H_2O)_6]^{2+}$ and $[Cu(H_2O)_6]^{2+}$ complexes it is observed that axial metal-oxygen distances ($M\text{-}O_{ax}$) are longer (by 0.3 Å) than the equatorial ones ($M\text{-}O_{eq}$), revealing the typical Jahn-Teller distortions associated to their electronic structure in the ground state. [43] BCP properties indicate that M-O equatorial bonds can be considered stronger as axial bond lengthening is accompanied by ρ_b diminution. Much weaker geometrical distortions (up to 0.05 Å) are shown by high spin $[Fe(H_2O)_6]^{2+}$ and $[Co(H_2O)_6]^{2+}$ complexes. Excluding Mn(II) and Ca(II) complexes, M-O distances are significantly longer when hexa-coordinated than in their tetracoordinated counterparts (Table S1).

3.2. Most stable structures for Cyanin-Metal hydrated complexes

As mentioned above, we have concentrated our study on 1:1 M:Cy complexes. Thus, models for $[MCy(H_2O)_{w-2}]^{(n-1)+}$ species (where Cy^- replaces two metal coordination sites) with w= 4, and 6 were optimized. Pseudo tetrahedral (***T*-4**) and square-planar (***SP*-4**) initial dispositions for the ligands were optimized for $[MCy(H_2O)_2]^{(n-1)+}$ models, whereas octahedral (***OC*-6**) initial geometry was considered for $[MCy(H_2O)_4]^{(n-1)+}$ ones. All of them were submitted to complete optimizations, with no symmetry restrictions, in the aqueous solution simulated with PCM. Only some of these initial structures were successfully located (Table 1). In order to assess the relative stability of the different complexes obtained for each of the metals tested in this study, we notice that while energies for ***SP*-4** and ***T*-4** structures can be compared directly, complexes with different coordination number require CP for BSSE. [41] They were made considering the partial dissociation processes given by equation (2).

$$[MCy(H_2O)_w]^{(n-1)+}\ (aq) \rightarrow [MCy(H_2O)_{w-2}]^{(n-1)+}\ (aq) + 2\ H_2O\ (aq) \qquad (2)$$

We have firstly noticed that the replacement of two water molecules by one Cy^- bidentate ligand modifies the coordination preference of some of the metals tested. This is the case for Cr(II) and Cu(II). For them, the most stable water complex is the hexaaqua but when coordinated to Cy^- the preferred geometry (Table 1) turns to be ***SP*-4**. Indeed, Cu(II) is the unique metal for which only one of the forms explored, ***SP*-4**, is found. For the remaining metals, the pseudo ***OC*-6** form is favored over pseudo ***T*-4** or ***SP*-4**. It can also be inferred from Table 1 that for most of the metal-complexes, relative energies for a second structure are significantly high pointing to they exist as only one form.

Table 1. Most stable structures found for the Cyanin-Metal hydrated complexes here studied. CP-corrected relative energies (in kcal mol^{-1} and obtained with PCM B3LYP/6-31++G(d,p) optimizations, including Grimme's dispersion correction) with regard to the most stable structure, Form 1, for each case are shown in parenthesis. Spin states are indicated (when S≠0) as superindices (e.g. ***T*-4**^{3} denotes the triplet state (S=1) for ***T*-4** structure).

Cation	Form 1	Form 2	Form 3
Na^+	***OC*-6**	***T*-4** (1.38)	***SP*-4** (1.44)
Mg(II)	***OC*-6**	**T-4** (13.47)	----
Al(III)	***OC*-6**	***T*-4** (34.55)	----
K^+	***OC*-6**	***T*-4** (1.25)	***SP*-4** (1.43)
Ca(II)	***OC*-6**	***T*-4** (8.58)	***SP*-4** (8.91)
Cr(III)	***OC*-6**^{4}	***SP*-4**^{4} (23.14)	----
Cr(II)	***SP*-4**^{5}	***OC*-6**^{3} (4.66)	----
Mn(II)	***OC*-6**^{6}	***T*-4**^{6} (6.31)	***SP*-4**^{4} (33.24)
Fe(III)	***OC*-6**^{6}	***SP*-4**^{6} (15.04)	***T*-4**^{4} (15.12)
Fe(II)	***OC*-6**^{5}	***SP*-4**^{5}(9.74)	----
Co(III)	***OC*-6**^{5}	***T*-4**^{3} (13.42)	***SP*-4**^{5} (13.54)
Co(II)	***OC*-6**^{4}	***T*-4**^{4} (7.51)	***SP*-4**^{2} (18.02)
Ni(II)	***OC*-6**^{3}	***T*-4**^{3}(14.32)	***SP*-4** (19.79)
Cu(II)	***SP*-4**^{2}	----	----
Zn(II)	***OC*-6**	***T*-4** (7.15)	***SP*-4** (8.15)

Concerning 1:2 metal-cyanin complexes, we have explored the effect of the replacement of four water molecules in $[Fe(H_2O)_4]^{3+}$ and $[Fe(H_2O)_6]^{3+}$ by two Cy^- units leading to high spin ***SP*-4** $[FeCy_2]^+$ and ***OC*-6** $[FeCy_2(H_2O)_2]^+$ complexes, respectively (Scheme 3). In ***SP*-4** $[FeCy_2]^+$, two possible arrangements of the two Cy^- ligands might be conceived: that where Fe-O3' (Fe-O4') bonds of both Cy^- ligands are in *cis* and that with Fe-O3' (Fe-O4') bonds in *trans*. In ***OC*-6** $[FeCy_2(H_2O)_2]^+$, we have, in addition, other

two possibilities considering the *syn*/*anti* relative position of the two remaining water molecules. Computed energies indicate that ***SP*-4** isomers are nearly isoenergetic (ΔE= 0.11 kcal·mol^{-1}) while energies for ***OC*-6** isomers were found to be within a range of 2 kcal·mol^{-1}. Moreover, ***OC*-6** coordination is 13.18 kcal·mol^{-1} more favorable than ***SP*-4**, very similar to what we have computed for the 1:1 stoichiometry ratio.

a)

***SP*-4**

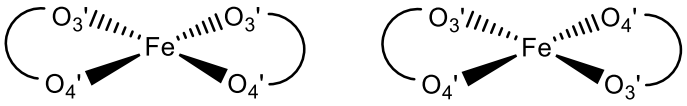

(0.00) *(0.11)*

b)

***OC*-6**

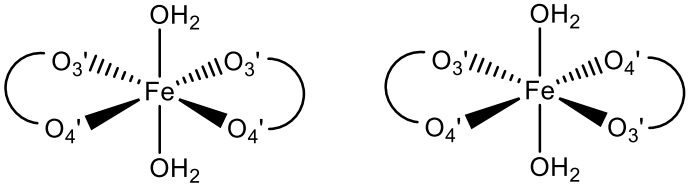

(2.11) *(2.61)*

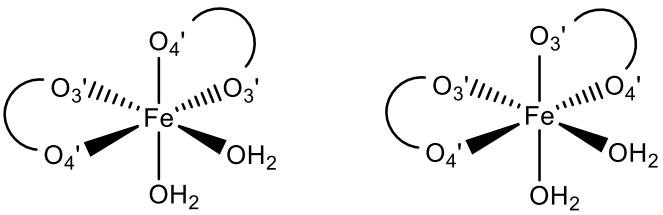

(0.00) *(0.54)*

Scheme 3. Regioisomers of 1:2 Fe(III):Cy^{-} complex explored in this work, with coordination numbers a) ***SP*-4** and b) ***OC*-6.** Energy difference (in kcal·mol^{-1}) in *(italics)* with regard to the most stable isomer of each coordination number.

3.3. Metal binding Cyanin affinities

Metal-binding affinities, $\Delta_b E$, (derived from thermally corrected electronic energies) for cyanin were computed making use of the complex formation process (3), which was applied to the most stable structure for each case (Table 1). CP corrections were carried out considering: i) two fragments for the model complex, the Cy^- model and the $[M(H_2O)_{w-2}]^{n+}$ fragment; and ii) three fragments for the $[M(H_2O)_w]^{n+}$ cation, two of the water molecules and the $[M(H_2O)_{w-2}]^{n+}$ fragment including the two water molecules displaying the closest disposition to that adopted in $[MCy(H_2O)_{w-2}]^{(n-1)+}$.

$$[M(H_2O)_w]^{n+}\,(aq) + Cy^-\,(aq) \rightarrow [MCy(H_2O)_{w-2}]^{(n-1)+}\,(aq) + 2\,H_2O\,(aq) \qquad (3)$$

Looking at $\Delta_b E$ values collected in Table 2, we can observe that the largest affinities (up to -108.06 kcal·mol^{-1}) correspond to binding with those metals in a higher oxidation state and that the affinity of Cy^- for a metal ion enhances as the number of electrons of the metal increases: Al(III) < Cr(III) < Fe(III) < Co(III). Also, binding with trivalent metals are significantly larger (by more than 30 kcal·mol^{-1}) than those computed with the same metal in the lower oxidation state (II). To sum up, both results indicate that M^{n+}:Cy^- interaction and stability increases as the number and charge of the M^{n+} rise. In line, higher $\Delta_b E$ values pretty well correlate with binding to metal ions bearing a larger acid character (lower pK_a, Table 2).

Table 2. Binding energies, $\Delta_b E$, (in kcal mol^{-1} and computed according to equation 3) for the most stable structures of the metal-cyanin hydrated complexes here studied. Electron densities at metal complexation BCPs, ρ_b, (all values in au multiplied by 10^3) and M-O bond lengths, R, (in Å) are also shown. See Figure 1 for nomenclature.

Cation		**B1**	**B2**	**B3**	**B4**	**B5**	**B6**	$\Delta_b E$	pK_a [44]
Na^+	ρ_b	24.2	20.5	8.6	13.5	14.4	11.9	-12.21	13.9
	R	2.272	2.338	2.663	2.488	2.464	2.530		
K^+	ρ_b	18.4	15.8	12.8	12.7	13.1	13.1	-6.36	14.0
	R	2.705	2.772	2.832	2.834	2.826	2.826		
Mg(II)	ρ_b	43.3	39.0	29.5	29.4	27.5	27.9	-25.26	11.2
	R	2.022	2.061	2.135	2.137	2.170	2.163		
Ca(II)	ρ_b	36.4	31.5	24.7	22.8	23.1	24.7	-17.62	12.7
	R	2.357	2.417	2.481	2.526	2.524	2.493		
Cr(II)	ρ_b	90.1	82.5	-----	-----	54.8	53.1	-42.46	5.5
	R	1.959	1.989	-----	-----	2.106	2.118		
Mn(II)	ρ_b	75.4	57.7	39.4	40.3	44.4	37.7	-30.69	10.6
	R	2.045	2.163	2.305	2.297	2.248	2.324		
Fe(II)	ρ_b	90.4	59.4	39.0	45.4	50.4	45.4	-32.40	9.4
	R	1.963	2.135	2.297	2.212	2.175	2.228		
Co(II)	ρ_b	83.3	66.9	45.6	49.0	49.7	53.9	-31.26	9.7
	R	1.988	2.074	2.218	2.180	2.170	2.141		
Ni(II)	ρ_b	84.2	77.9	52.4	51.6	54.1	53.9	-32.40	9.9
	R	1.977	2.004	2.145	2.142	2.124	2.126		
Cu(II)	ρ_b	107.6	101.2	-----	-----	71.4	71.8	-52.04	8
	R	1.888	1.911	-----	-----	2.020	2.016		
Zn(II)	ρ_b	86.5	74.4	45.2	41.8	51.7	52.7	-31.74	9.0
	R	1.983	2.046	2.226	2.264	2.175	2.163		
Al(III)	ρ_b	79.5	75.1	46.1	46.1	51.3	51.1	-63.42	5.0
	R	1.819	1.840	1.991	1.990	1.955	1.959		
Cr(III)	ρ_b	116.5	109.3	66.2	66.8	62.1	62.1	-72.62	3.7
	R	1.882	1.903	2.046	2.042	2.071	2.067		
Fe(III)	ρ_b	89.5	82.0	52.4	52.6	59.5	54.3	-80.64	2.2
	R	1.969	2.009	2.169	2.163	2.114	2.151		
Co(III)	ρ_b	70.9	70.4	52.2	53.5	54.9	54.8	-108.66	0.5
	R	2.046	2.050	2.152	2.150	2.132	2.128		
Fe(III)[a]	ρ_b	96.10	81.09	97.95	78.62	48.94	47.98	-41.94[b]	
	R	1.950	2.018	1.943	2.035	2.212	2.220		

[a] See Fig. 3.

[b] Binding energy was obtained according to equation $FeCy(H_2O)_4]^{2+} + Cy^- \rightarrow [FeCy_2(H_2O)_2]^+ + 2H_2O$

To the best of our knowledge, data concerning metal-anthocyanin association or stability constants are very scarce. [19,32-34] This contrasts to the larger number of works dedicated to anthocyanin self-association and flavonoid/anthocyanin association constants. [9] However, some of our $\Delta_b E$ values can be pretty well compared with the experimental data available. In particular, our results indicate a larger stability of the metal-cyanin complex with Cu(II), $\Delta_b E$ = -52.04 kcal·mol^{-1}, than with Zn(II), $\Delta_b E$ = -31.74 kcal·mol^{-1}, in agreement with what has been observed experimentally. [33] Also, it has been found [29] that binding to Fe(II) goes more slowly than with Fe(III) and that complexation with the latter goes faster than with Al(III), which can be pretty well correlated with our results.

Second replacement of two water molecules by Cy^- ligand results in a less favorable process. When a second Cy^- ligand replaces two water molecules in $[FeCy(H_2O)_4]^{2+}$ leading to $[FeCy_2(H_2O)_2]^+$ the binding energy (-41.94 kcal·mol^{-1}) indicates this substitution is significantly less feasible than the first one (-79.62 kcal·mol^{-1}). This result would be in agreement with experimental evidences remarking the larger population of 1:1 species. Moreover, this result is in line with what we found previously for Al(III) and Mg(II), [20] that is, that subsequent water replacement by Cy^- results in a less energetically favored process.

A more environmental-related result is that Cy^- displays significant affinity for cations which are usually considered of potential risk. For instance, its affinity for Cr(III) and Al(III) exceeds that shown for Mg(II), the cation which is expected to be attached to Cy^- in unpolluted plant environments, promoting the Mg(II)/Al(III) and Mg(II)/Cr(III) replacement mechanism. In general, we notice that affinities for all the metals tested, but Na^+, K^+ and Ca(II), are from slightly to very higher than that for Mg(II).

3.2. Molecular structure metal-cyanin complexes

As shown in Figure 1, Cy^- acts in all the metal complexes as a bidentate ligand giving rise to a five-membered ring, whose ring critical point (RCP, Figure 1) is always found by the QTAIM electron density analysis. Two features that can be used in order to estimate the geometry distortions associated to complex formation are: i) the bite distance (O3'···O4' interatomic distance); and ii) The M-O bond lengths with water molecules. The bite distance shrinks significantly in most of the complexes (up to 0.223 Å) with regard to the solvated Cy^-. Alkaline cations are the unique exceptions where this distance changes below 0.05 Å. M-O_W distances with the same coordination number (pseudo ***OC*-6** structures) are also longer in $[MCy(H_2O)_4]^+$ than in $[M(H_2O)_6]^{2+}$.

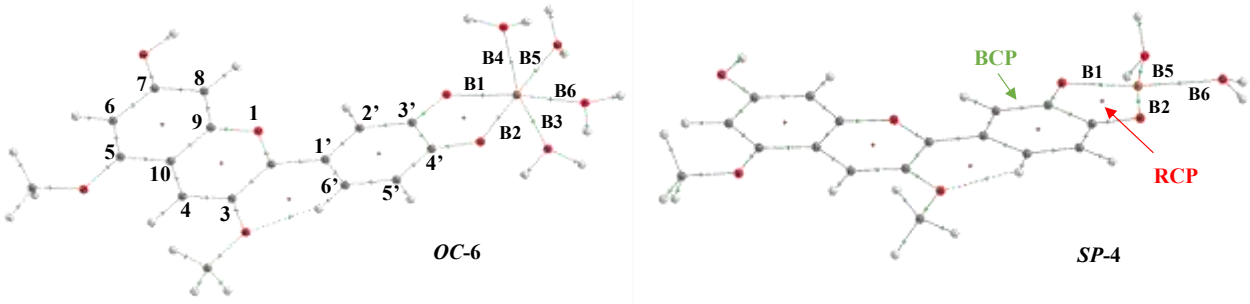

Fig. 1. ***OC*-6** and ***SP*-4** structures for $[MCy(H_2O)_{w-2}]^{(n-1)+}$ complexes. IUPAC atom numbering for the skeleton of cyanin model is shown in ***OC*-6** structure. Green and smaller red balls indicate, respectively, bond (BCP) and ring (RCP) critical points. B1-B6 labels are used to indicate BCPs between metal and oxygen 3' and 4' of cyanin, M-O_{Cy}, or oxygen atoms of water molecules, M-O_w.

Metal complexation modifies the geometry of Cy^- with regard to the aqueous solvated anionic ligand. In particular, C3'-O3' and C4'-O4' bonds become largely elongated as much as 1.372 and 1.358 Å, respectively, after complexation (1.287 and 1.258 Å, respectively, in free Cy^- ligand). Yet, C3'-O3' is always longer than C4'-O4'. In

344 $[FeCy_2(H_2O)_2]^+$, C3'-O3' and C4'-O4' bonds of both Cy ligands are equivalent with C-
345 O3' bond distances (1.334 Å) being still larger than those of C-O4' (1.304 Å). They are
346 as well longer that those in $[FeCy(H_2O)_4]^{2+}$ ($d_{C\text{-}O3'}$: 1.311 Å, $d_{C\text{-}O4'}$: 1.297 Å). This is
347 noticeable by looking at $\Delta\rho_b$ values in Figure 3 where we can see there is a reduction of
348 electron density at C-O3' and C-O4' bonds when Cy^- is in the complex, being this
349 reduction increased in the 1:2 complex formation.
350 In terms of the resonance model, the dienolate form II (Scheme 2) seems to be more
351 favored in the complex than in free Cy^- ligand if we exclude Na^+ and K^+ complexation.
352 This can also be observed in the C2-C1' bond length (Table 3), which lengthens from
353 0.007 Å in Ca(II) complex to 0.042 Å and 0.045 Å in Fe(III) and Co(III) complexes,
354 respectively, while it remains unchanged in Na^+ and K^+ compound, in line with a weak
355 complexation. These geometrical trends are reflected by the QTAIM properties. Thus,
356 bond lengthening is accompanied by ρ_b diminution (Table 3) and corresponding
357 reductions of the absolute values of $\nabla^2\rho_b$ and H_b, pointing to a weaker and less covalent
358 bonds.
359
360
361
362
363
364
365
366
367
368
369

Table 3. C2-C1' bond distance, R, (in Å) in the most stable structures for the most stable form of the diverse metal-cyanin hydrated compounds here studied and corresponding ρ_b, $\nabla\rho_b$ and H_b values (in au multiplied by 10^3, 10^2 and 10, respectively).

M	R(C2-C1')	ρ_b(C2-C1')	$\nabla\rho_b$	H_b
Cy^- [a]	1.406	306.4	-82.95	-3.09
Na^+	1.408	305.2	-82.70	-3.07
Mg(II)	1.418	300.3	-81.09	-2.98
Al(III)	1.438	291.0	-77.30	-2.79
K^+	1.407	305.7	-82.80	-3.08
Ca(II)	1.413	303.0	-82.03	-3.03
Cr(III)	1.440	290.1	-76.89	-2.77
Cr(II)	1.425	296.9	-79.71	-2.91
Mn(II)	1.419	300.1	-80.97	-2.98
Fe(III)	1.448	286.6	-75.35	-2.69
Fe(II)	1.419	300.3	-80.99	-2.98
Co(III)[b]	1.451	285.4	-74.88	-2.65
Co(II)	1.420	299.5	-80.71	-2.96
Ni(II)	1.421	299.1	-80.56	-2.96
Cu(II)	1.430	294.6	-78.78	-2.87
Zn(II)	1.420	299.4	-80.71	-2.96
Fe(III)[b]	1.430	294.8	-78.82	-2.87

[a] Taken from the geometry of the parent Cy^- uncomplexed anion in PCM modelled aqueous solution. [b] In the most stable $[FeCy_2(H_2O)_2]^+$ complex. [b] Complexation of Cy^- with Co(III) makes Cy^- to lose co-planarity between AC and B rings (dihedral angle of 14º).

Indeed, the variations experienced by ρ_b values in C2-C1' are highly correlated (r^2 =0.999) with their bond lengths along the series of complexes here studied (Fig. 2). As

well, we have found that the longer the C2-C1' distance (smaller ρ_b) the larger the binding energy (Table 3) with a pretty well correlation (r^2 = 0.971; they become better correlated, r^2 = 0.991, when Co(III) is excluded).

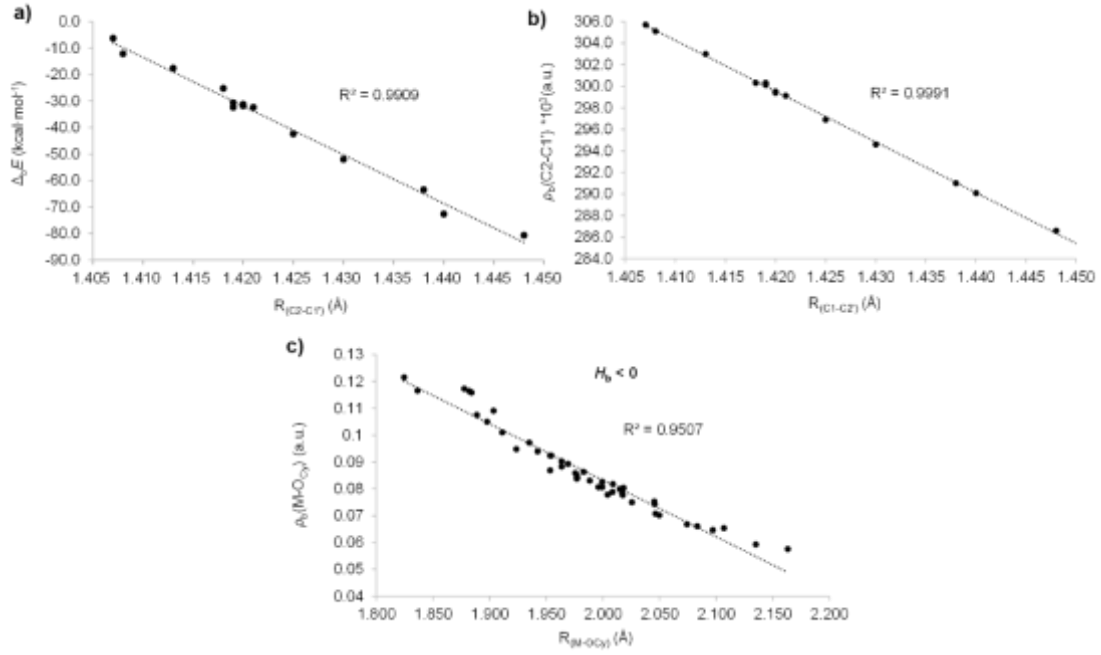

Fig. 2. Correlation found between a) binding energies, $\Delta_b E$, in kcal·mol^{-1}, for metal-Cy complexes and their corresponding C2-C1' bond distance, $R_{(C2-C1')}$, (in Å); b) BCP electron density, ρ_b, at C2-C1' and $R_{(C2-C1')}$ and c) ρ_b at M-O$_{Cy}$ and $R_{(M-OCy)}$, for complexes featuring H_b <0 (at M-O$_{Cy}$ BCP).

M-O3' and M-O4' bonds lengths span along a wide interval ranging from 1.75 to 2.77 Å (B1 and B2, respectively, see Fig. 1 and Table 2). In all complexes, M-O3' bonds are stronger than M-O4' ones, according to shorter bond lengths and larger ρ_b values. Further, the values of the total energy density at the BCP (Table S2) are small and negative (H_b < 0) for most of these bonds, revealing the hallmarks of bonding to a metal atom. In contrast, the positive H_b values observed in complexes of Na^+, K^+, Mg(II), Ca(II), and Al(III) complexes, show their M···O interactions are established between closed shells, like in

ionic interactions. Bearing in mind the pattern followed by covalent contributions to the bonding of metals in protein structures: [45] $K^+ < Na^+ < Ca^{2+} < Mn^{2+} < Fe^{2+} < Co^{2+} \sim Ni^{2+} \sim Cu^{2+} > Zn^{2+}$; H_b values pretty well reproduce the series. Besides, when bonds with positive and negative H_b values are considered separately, ρ_b values and bond distances display a fairly good linear correlation especially (Fig. 2), for M-O_{Cy-} bonds of metal-cyanin complexes with $H_b < 0$.

It could be expected that larger binding affinities should be related to larger values of the $\rho(\mathbf{r})$ at the M-O BCPs. Nevertheless, ρ_b values can only be compared within a series of bonds established by the same pair of elements. [27,28] In the three cases where ρ_b values can be compared, that is when an oxidation number differs for the same pair of atoms (Co, Fe and Cr complexes), we observe (Table 2) the largest binding energy does correspond (when summing up the six ρ_b (M-O) values) to the strongest metal-oxygen bonds. A clearer structural trend we can infer from ρ_b data is that, excluding, alkaline and Ca(II) cations, M-O bonds with Cy^- are significantly stronger than those established with water molecules.

QTAIM atomic charges of the Cy^- ligand become reduced in the complexation process, as exemplified in Figure 3 for ***OC-6*** $[FeCy(H_2O)_4]^{2+}$ and $[FeCy_2(H_2O)_2]^+$ formation (the carbons of the methoxyl groups bonded to C5 and C3, C3' and C4' are exceptions to this rule. The reasons for these exceptions can be found considering the same scheme proposed for explaining electron density reorganization in molecular protonations). [46,47] Moreover (Tables 2 and 4), the results indicate that the larger the net charge transfer (CT), from Cy^- to the metal cation, the more favored the metal-complex formation (the higher binding energy, $\Delta_b E$). Also, we notice (see Table S3) that coordination number partially modified this trend, as water molecules contribute in reducing the positive charge of the metal and thus, the higher the coordination number the lower CT from Cy^-.

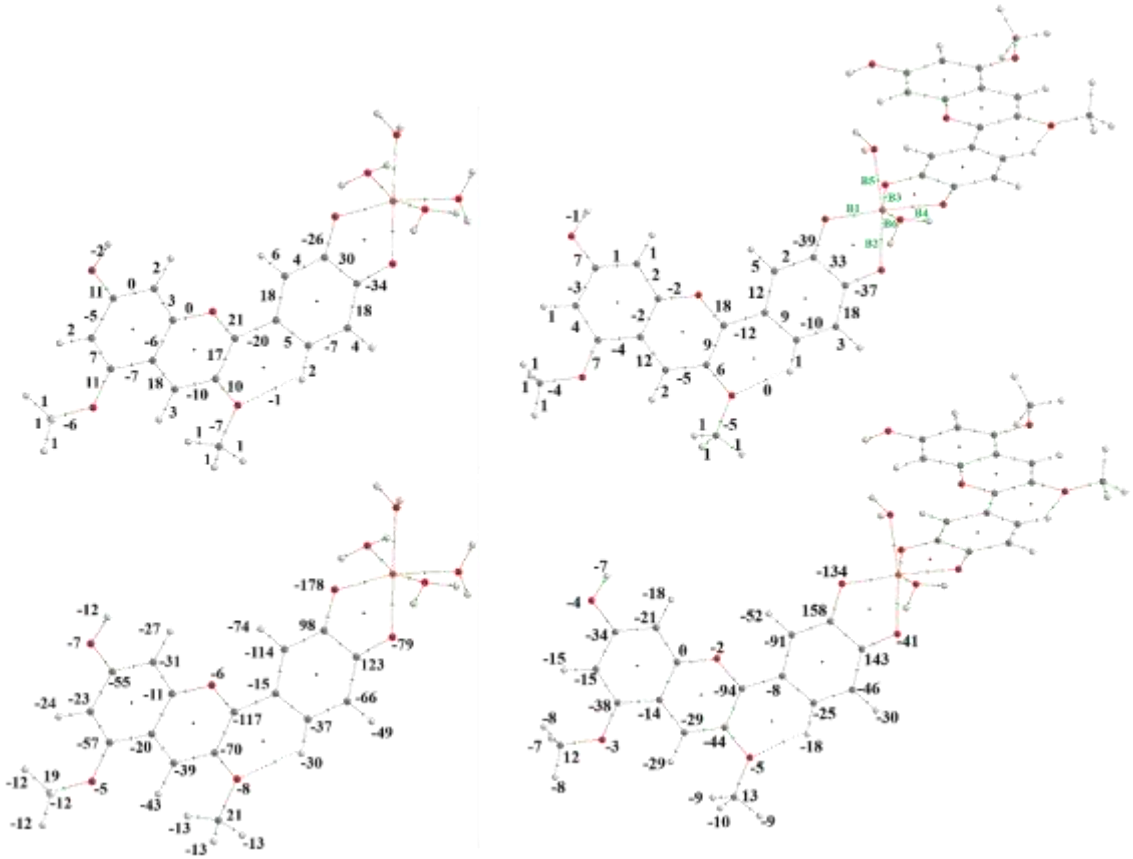

Fig. 3. $\Delta\rho_b$ values (top) and $\Delta Q(\Omega)$ QTAIM atomic charges (bottom), in au multiplied by 10^3, for PCM optimized structures of the most stable 1:1 (left) and 1:2 (right) Fe(III):Cyanin complexes.

Looking at Table 4 in more detail, we notice that, upon metal complexation, charge density (CD) is displaced mainly from the AC system (chromenylium fragment) to the metal moving through the B ring, whose partial charge remains nearly constant (when compared with the reference **A3'4'**). This is true except for Cu(II) and M(III) complexes where electron density of the B ring starts being significantly transferred to the metal. For example, upon formation of $[CoCy(H_2O)_4]^{2+}$ CD moves from the whole ligand (0.71 e^- from AC and 0.55 e^- from B) to the metal which largely reduces its positive charge (by 1.60 e^-).

Table 4. QTAIM atomic charges summed up into atomic groups (Cy, H_2O's, B (B-ring), AC (AC-rings)) for the most stable structures of the cationic (**C**), neutral (**N4'** and **N7**), and anionic (**A3'4'** and **A74'**) forms of the cyanidin-3,5-di-O-methyl and their metal-complexes studied here. QTAIM atomic charge of the metal, Q(M), is also shown.

	$\sum Q(\Omega^{Cy})$	$\sum Q(\Omega^{H2O's})$	Q(M)	$\sum Q(\Omega^{B})$	$\sum Q(\Omega^{AC})$
C	+1	---	---	0.360	0.640
N4'	0	---	---	-0.313	0.313
N7	0	---	---	0.221	-0.221
A74'	-1	---	---	0.586	-1.586
A3'4'	-1	---	---	-1.051	0.0510
Na^+	-0.9442	0.0359	0.9068	-1.0678	0.1237
K^+	-0.9563	0.0345	0.9227	-1.0450	0.0887
Mg(II)	-0.8691	0.0941	1.7741	-1.1754	0.3064
Ca(II)	-0.8996	0.0967	1.8016	-1.1249	0.2253
Cr(II)	-0.6293	0.1558	1.4733	-1.0195	0.3902
Mn(II)	-0.7287	0.1990	1.5304	-1.0449	0.3162
Fe(II)	-0.6759	0.2468	1.4292	-1.000	0.3245
Co(II)	-0.6406	0.2929	1.3474	-0.9762	0.3357
Ni(II)	-0.6165	0.3604	1.2562	-0.9552	0.3387
Cu(II)	-0.4201	0.2553	1.1626	-0.8661	0.4460
Zn(II)	-0.6420	0.3074	1.3356	-0.9765	0.3345
Al(III)	-0.7712	0.1985	2.5724	-1.2913	0.5200
Cr(III)	-0.3358	0.4740	1.8622	-0.8792	0.5434
Fe(III)	0.0152	0.3470	1.6391	-0.6295	0.6446
Co(III)	0.2593	0.3515	1.3904	-0.4518	0.7111

It is worth mentioning the particular case of $[CyAl(H_2O)_4]^{2+}$ where despite the large charge density depletion in AC (0.52 e^-), in the complexation process, this is not translated into CT to the metal but partially accumulated in B. As a result, the metal cation reduces its positive charge by only 0.43 e^- (which includes the contribution of water molecules in reducing the positive charge of the metal, ca. 0.20 e^-).

3.3.Optical properties of metal-Cyanin complexes

It is well-known that anthocyanidins show light absorption in the visible region offering from red to blue color depending on the pH, that is, depending on the colored form present in the mixture: the cation (red) in acid solutions, neutral (violet or purple) in neutral solutions, and the anion (blue) in alkaline pH. As a result, the visible absorption band shift to longer wavelengths when increasing pH.

As it was mentioned in the Introduction section, metal complexation might shift the pH equilibria towards the anion form (Scheme 1) contributing to the persistence of pigmentation at pH values where otherwise anthocyanins would suffer from hydration and thus, discoloration. Therefore, the visible absorption band might also shift to longer wavelengths upon complexation with metal ions.

Thus, we were keen on the ability of metal-anthocyanins to absorb UV wavebands, whether the strength of the binding play a role and the nature of the electronic transition. To shed light into these questions, the vertical singlet electronic transition energies were computed by means of single point calculations at TD/B3LYP/6-31++G(d,p)/PCM level employing fully optimized geometries in implicit solvent (water) model. Calculations at the same level were done on the different colored species of cyanin depending on pH, in order to analyze the difference, if so, upon metal complexation (*e.g.*, whether or not complexation originates a bathochromic shift).

In Fig. 4 is depicted the merged UV-Vis spectra for the most stable cation (**C**), neutral (**N4'** and **N7**) and anion (**A74'**) species of cyanidin-3,5-diO-methyl. [31] All of these species absorb in the visible region where maximum visible wavelength is shifted to longer wavelengths (the common sign of more conjugated chromophore system leading to smaller HOMO-LUMO gaps, Δ_{H-L}) on going from cation (494.8 nm, f=0.5402; Δ_{H-L}: 2.84 eV) to the most stable anion (552.8 nm; f=0.8263; Δ_{H-L}: 2.41 eV) of cyanin, with increasing oscillator strength. In contrast, the **A3'4'** anionic form displays two absorption bands in the visible region, the longest absorption wavelength at 648.38 nm (f=0.3877;

479 Δ_{H-L}: 2.08 eV) but the one with the highest molar extinction coefficient arises at 428.8

480 nm (f=0.6041).

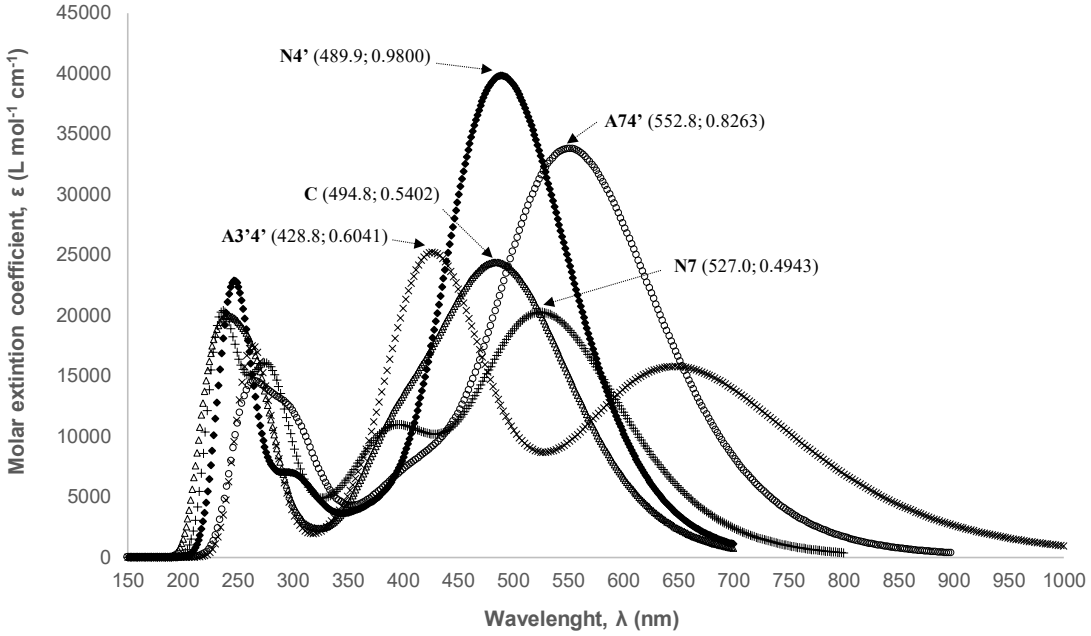

481

482 Fig. 4. UV-visible spectra of the different colored forms of cyanidin-3,5-O-methy:

483 cation, **C**, neutral (**N4'** and **N7**) and anion (**A74'** and **A3'4'**) computed at the

484 TD/B3LYP/6-31++G**/PCM(water)// B3LYP/6-31++G**/PCM(water) level of theory.

485 In brackets, λ_{max} and corresponding oscillator strength are shown.

486

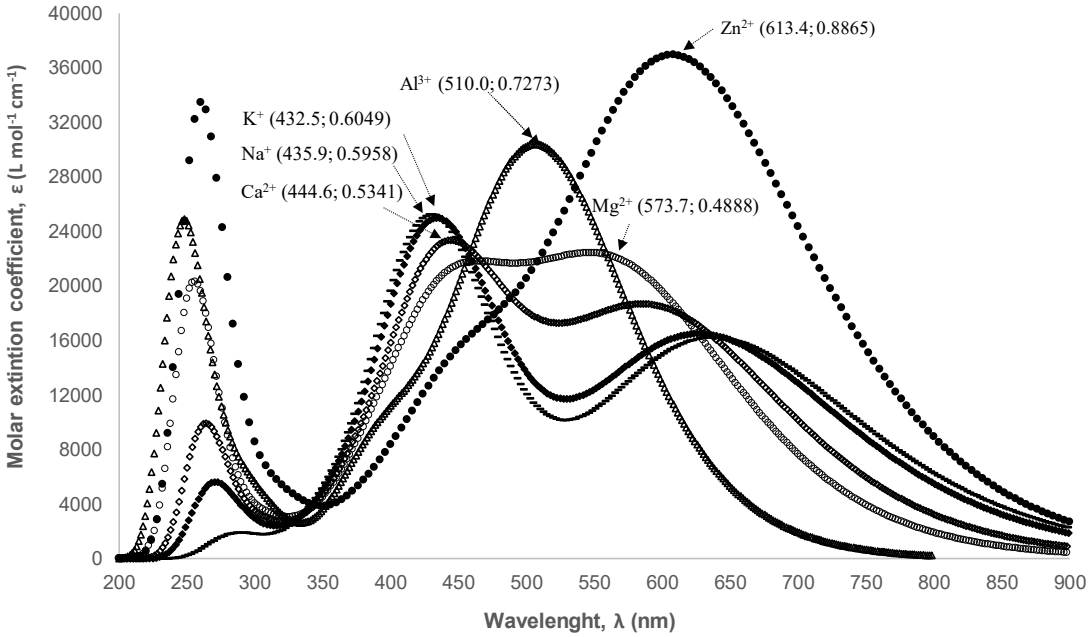

Fig. 5. UV-visible spectra for closed-shell metal-cyanin complexes studied here computed at the TD/B3LYP/6-31++G**/PCM(water)// B3LYP/6-31++G**/PCM(water) level of theory. In brackets, λ_{max} and corresponding oscillator strength are shown.

When looking at the UV-Vis spectra of the closed-shell metal-complexes depicted in Fig. 5, we notice that for K^+, Na^+ and Ca(II) the UV-Vis spectra are reminiscent of that of **A3'4'** which is in line with the weak coordination and the larger participation of the enolate form I. Comparing with the absorption spectrum of **A3'4'**, we observe that on going from K^+, Na^+ to Ca(II) up to Mg(II) the longest wavelength (assigned to a HOMO→LUMO transition) is blue shifted accompanied of a hyperchromic effect. Reversibly, the wavelength with larger oscillator strength in the visible region (associated with a HOMO-1 to LUMO electronic transition) is red shifted together with a hypochromic effect (on going from K^+ to Mg(II)). Indeed, in Mg(II)-complex both excitation energies feature comparable strengths: 573.7 nm (f = 0.4888) and 449.6 nm (f = 0.4395). Chelation with Al(III) and Zn(II) provides different UV-vis spectra, where both metal complexes display one strong absorption band in the visible region (Fig. 5).

Indeed, Zn(II) complex displays the largest bathochromic as well as the largest hyperchromic effects of these series of complexes.

For open-shell systems, TD-DFT often produces physically meaningless excited states due to heavy spin contaminations. Thus, the analysis of the results obtained for the open-shell metal-cyanin complexes studied here, needs to be done carefully and taken as a first approach to their optical properties.

We have concentrated on those complexes whose UV-vis spectra displays one strong band in the visible region at longer wavelength than free cyanin and whose oscillator strengths f larger than 0.5 and that do not suffer from spin contamination. Five of them fulfill these conditions. They are those of Fe(II), Fe(III), Co(II) and Cu(II). Their corresponding maximum absorption wavelength, excitation energies and oscillator strength are collected in Table 5. All of them show a bathochromic wavelength shift with respect to the complex with Al(III) (510.0 nm, 2.43 eV).

Table 5. Excitation wavelengths, λ, (in nm), corresponding excitation energies, EE, (in eV) and oscillator strength, f, for selected open-shell transition metal complexes of cyanin. Spin contamination, $<S^2>$, of the transition is also shown.

	Cr(III)	Fe(II)	Fe(III)	Co(II)	Cu(II)
λ (nm)	516.5	541.7	535.5	562.0	534.2
f	0.7224	0.6200	0.5213	0.5515	0.5008
EE (eV)	2.40	2.29	2.32	2.21	2.32
$<S^2>$	3.828	6.064	8.921	3.838	0.759

Examination of the Frontier Molecular Orbitals (FMO) indicate the electronic π cloud distribution of HOMO´s in metal-cyanin complexes is largely localized on the cyanin moiety in close-shell complexes where CT is near negligible. This behavior partially

525 changes in transition metal complexes with increasing participation in HOMO of the
526 metal atom as CT increases (Table 4, Fig. 6). LUMO pattern in close-shell complexes is,
527 as well, spread over the cyanin dye with negligible contribution of the metal. This
528 behavior is consistent with the $\pi \rightarrow \pi^*$ electronic transition takes place mainly within the
529 dye (among B, A and C rings). In open-shell metal complexes, the contribution of the
530 metal ion in LUMO's starts to be significant, as exemplified by the Fe(III) complex (Fig.
531 6c) and the picture dramatically changes when looking at LUMO of the Cu(II) complex
532 (Fig. 6c) being fully localized at the metal fragment and surrounding oxygen atoms.

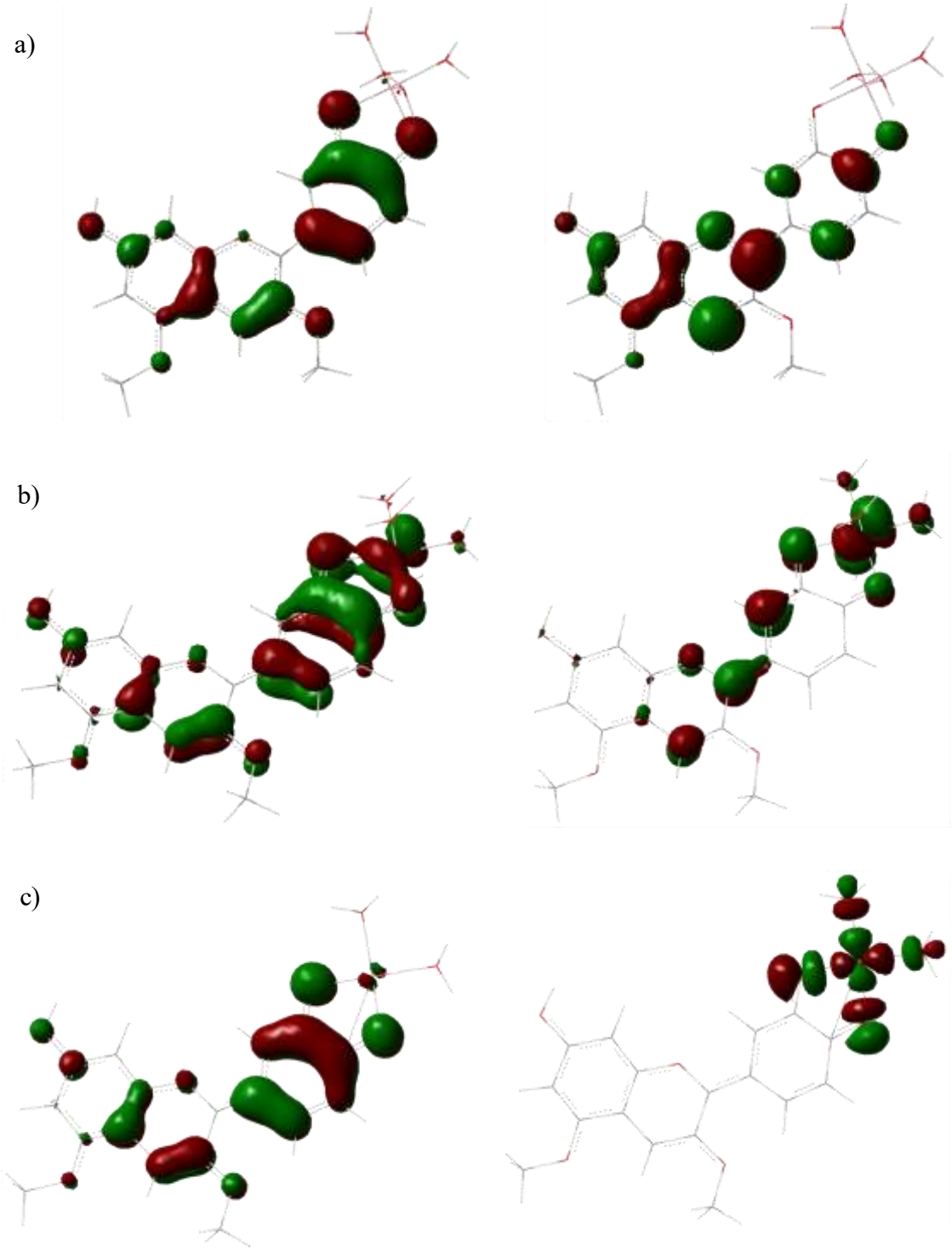

Fig. 6. Frontier Molecular Orbital for selected metal-cyanin complexes. Plots of ± 0.04 au isosurfaces for the HOMO (left) and LUMO (right) of a) $[CyAlw_4]^{2+}$, b) $[CyFew_4]^{2+}$ and c) $[CyCuw_2]^{+}$. Plots were made with Gaussview.

539 *3.4.Conclusions*

540

541 To the best of our knowledge, this is the first theoretical work on metal complexation
542 by cyanin where their geometries and corresponding electronic structure analysis have
543 been carried out by means of DFT and QTAIM. The ability of these metal complexes in
544 absorbing visible light has been investigated by means of TDDFT and further understood
545 by examination of their frontier molecular orbitals.

546 Complexation with metal ions by Cy^- leads to ligand to metal charge transfer (LMCT)
547 complexes where the higher the binding affinity the larger the charge transfer, CT, though
548 coordination number also play a role as water molecules also contribute to the reduction
549 of the positive charge of the metal ion. Upon metal complexation the Cy^- ligand molecular
550 structure is more compatible with a dienolate-like structure rather than the 4'-keto-
551 quinoidal-like structure which play a role in the shape of UV-vis spectra.

552 Examination of FMO allow us to describe their absorption in the visible region as
553 charge transfer $\pi \rightarrow \pi^*$ electronic transition within the dye moiety, except in the Cu(II)-
554 cyanin complex where LUMO is largely localized on the metal ion.

555 As HOMO to LUMO visible absorptions take place within the dye moiety, it must be
556 strongly affected by self-association or co-pigmentation with other colorless polyphenols.
557 Thus, future work would be dealt with the effect of the interaction with other polyphenols
558 on the ability to absorb visible light of these complexes.

559

560 **ACKNOWLEDGMENTS**

561 The authors thank "Centro de Supercomputación de Galicia" (CESGA) for free access to
562 its computational facilities, and financial support from Spanish Ministry of Economy and
563 FEDER through research project CTQ2010-21500. L.E. thanks Xunta de Galicia for

564 financial support through the I2C program and associated funded project (POS-
565 B/2016/002).

REFERENCES

[1] Shibata K, Shibata Y, Kasiwagi I. Studies on Anthocyanins: Color Variation in Anthocyanins J Am Chem Soc 1919; 41: 208-220.

[2] Goto T, Kondo T. Structure and Molecular Stacking of Anthocyanins – Flower Color Variation. Angew Chem Int Ed Engl 1991; 30: 17-33.

[3] Yoshida K, Mori M, Kondo T. Blue flower color development by anthocyanins: from chemical structure to cell physiology. Nat Prod Rep 2009; 26: 884–915.

[4] Pina F, Oliveira J, de Freitas V. Anthocyanins and derivatives are more than flavylium cations. Tetrahedron 2015; 71: 3107-3114.

[5] (a) Dangles O, Elhabiri M, Brouillard R. Kinetic and thermodynamic investigation of the Aluminium-anthocyanin complexation in aqueous solution. J Chem Soc Perkin Trans 2 1994; 2587-2596. (b) Elhabiri M, Figueiredo P, Toki K, Saitoc N, Brouillard R. Anthocyanin–aluminium and –gallium complexes in aqueous solution. J Chem Soc Perkin Trans 2 1997: 355-362.

[6] Schreiber HD, Swink AM, Godsey TD. The chemical mechanism for Al^{3+} complexing with delphinidin: A model for the bluing of hydrangea sepals. J Inorg Biochem 2010; 104: 732–739.

[7] Mora-Soumille N, Al Bittar S, Rosa M, Dangles O. Analogs of anthocyanins with a 3',4'-dihydroxy substitution: Synthesis and investigation of their acid-base, hydration, metal binding and hydrogen-donating properties in aqueous solution. Dyes Pigm 2013, 96, 7-15.

[8] Sigurdson GT, Robbins C, Giusti MM. Effects of hydroxycinnamic acids on blue color expression of cyanidin derivatives and their metal. Food Chem 2017; 234: 131−138.

[9] Trouillas P, Sancho-García JC, De Freitas V, Gierschner J, Otyepka M, Dangles O. Stabilizing and Modulating Color by Copigmentation: Insights from theory and experiment. Chem Rev 2016; 116: 4937−4982.

592 [10] Sigurdson GT, Robbins C, Giusti MM. Evaluating the role of metal ions in the
593 bathochromic and hyperchromic responses of cyanidin derivatives in acidic and alkaline
594 pH. Food Chem 2016; 208: 26–34.
595 [11] (a) Cortez R, Luna-Vital DA, Margulis D, Gonzalez de Mejia E. Natural Pigments:
596 Stabilization Methods of Anthocyanins for Food Applications. Comp Rev Food Sci Food
597 Saf 2017; 16: 180-198. (b) Ratanapoompinyo J, Nguyen LT, Devkota L, Shrestha P. The
598 effects of selected metal ions on the stability of red cabbage anthocyanins and total
599 phenolic compounds subjected to encapsulation process. J Food Process Preserv 2017;
600 41: e13234.
601 [12] Wang H, Tang Z, Zhou W. A method for dyeing cotton fabric with anthocyanin dyes
602 extracted from mulberry (Morus rubra) fruits. Colora Technol 2016; 132: 222–231.
603 [13] Landi M, Tattini M, Gould KS. Multiple functional roles of anthocyanins in plant-
604 environment interactions. Environ Exp Bot 2015; 119: 4–17.
605 [14] Cheng GW, Crisosto CH. Iron-polyphenol Complex Formation and Skin
606 Discoloration in Peaches and Nectarines. J Am Soc Hort Sci 1997; 122: 95-99.
607 [15] Sigurdson GT, Giusti MM. Bathochromic and Hyperchromic Effects of Aluminum
608 Salt Complexation by Anthocyanins from Edible Sources for Blue Color Development. J
609 Agric Food Chem 2014; 62: 6955−6965.
610 [16] Buchweitz M, Gudi G, Carle R, Kammerera DR, Schulz H. Systematic investigations
611 of anthocyanin–metal interactions by Raman spectroscopy. J Raman Spectrosc 2012; 43:
612 2001–2007.
613 [17] Calogero G, Yum JH, Sinopoli A, Di Marco G, Grätzel M, Nazeeruddin MK.
614 Anthocyanins and betalains as light-harvesting pigments for dye-sensitized solar cells.
615 Solar Energy 2012; 86: 1563–1575.

616 [18] Fedenko VS, Shemet SA, Landi M. UV–vis spectroscopy and colorimetric models
617 for detecting anthocyanin-metal complexes in plants: An overview of in vitro and in vivo
618 techniques. J Plant Phys 2017; 212: 13–28.
619 [19] Marković JMD, Veselinović DS, Baranac JM, Brdarić TP. Spectroscopic and
620 theoretical study of cyanidin-aluminum (III) complexes. Spectrosc Lett 2008; 41: 104-
621 115.
622 [20] Estévez L, Otero N, Mosquera RA. Molecular structure of cyanidin metal
623 complexes: Al(III) versus Mg(II). Theor Chem Acc 2011; 128: 485-495.
624 [21] García-Bugarín M, Mosquera RA. On the structure of Zn(II) and Cu(II) cyanin
625 complexes in aqueous solution. Struct Chem 2014; 25: 1647-1657.
626 [22] Furia E, Marino T, Russo N. Insights into the coordination mode of quercetin with
627 the Al(III) ion from a combined experimental and theoretical study. Dalton Trans 2014;
628 43: 7269-7274.
629 [23] Leopoldini M, Russo N, Chiodo S, Toscano M. Iron chelation by the powerful
630 antioxidant flavonoid quercetin. J Agric Food Chem 2006; 54: 6343-6351.
631 [24] Primikyri A, Mazzone G, Lekka C, Tzakos AG, Russo N, Gerothanassis IP.
632 Understanding Zinc(II) chelation with quercetin and luteolin: a combined NMR and
633 theoretical study. J Phys Chem B 2015; 119: 83−95.
634 [25] Ferreira da Silva P, Lima JC, Freitas AA, Shimizu K, Macanita AL, Quina FH.
635 Charge-transfer complexation as a general phenomenon in the copigmentation of
636 anthocyanins. J Phys Chem A 2005; 109: 7329–7338.
637 [26] Pina F, Melo MJ, Laia CAT, Parola AJ, Lima JC. Chemistry and applications of
638 flavylium compounds: a handful of colours. Chem Soc Rev 2012; 41: 869–908.
639 [27] Bader RFW. Atoms in Molecules- A Quantum Theory; International Series of
640 Monographs in Chemistry, No 22, Oxford University Press: Oxford, 1990.

641 [28] Bader RFW. A quantum theory of molecular structure and its applications. Chem
642 Rev 1991; 91: 893-928.
643 [29] Al Bittar S, Mora N, Loonis M, Dangles O. Chemically Synthesized Glycosides of
644 Hydroxylated Flavylium Ions as Suitable Models of Anthocyanins: Binding to Iron Ions
645 and Human Serum Albumin, Antioxidant Activity in Model Gastric Conditions.
646 Molecules 2014; 19: 20709-20730.
647 [30] Shiono M, Matsugaki N, Takeda K. Phytochemistry: structure of the blue cornflower
648 pigment. Nature 2005; 436: 791-791.
649 [31] Estévez L, Mosquera RA. Conformational and Substitution Effects on the Electron
650 Distribution in a Series of Anthocyanidins. J Phys Chem A 2009; 113: 9908-9919.
651 [32] Moncada MC, Moura S, Melo MJ, Roque A, Lodeiro C, Pina F. Complexation of
652 aluminum(III) by anthocyanins and synthetic flavylium salts A source for blue and purple
653 color. Inorg Chim Acta 2003; 356: 51-61.
654 [33] Esparza I, Santamaría C, García-Mina JM, Fernández JM. Complexing capacity
655 profiles of naturally occurring ligands in Tempranillo wines for Cu and Zn: an
656 electroanalytical approach for cupric casse. Anal Chim Acta 2007; 599: 67-75.
657 [34] Smyk, B.; Pliszka, B.; Drabent, R. Interaction between Cyanidin 3-glucoside and
658 Cu(II) ions. Food Chem 2008; 107: 1616–1622.
659 [35] Xu Z. Mechanics of metal-catecholate complexes: The roles of coordination state
660 and metal types. Sci Rep 2013; 3: 2914.
661 [36] Salinas I, Esparza I, Gomez S, Santamaria K, Fernandez JM. A Study of Heavy Metal
662 Complexation in Grape Juice. Electroanal 2005; 17: 469–475.
663 [37] Tomasi, J.; Mennuci, B.; Cammi, R. Quantum mechanical continuum solvation
664 models. Chem Rev 2005; 105: 2999-3093.
665 [38] Gaussian 09, Revision D.01, Frisch MJ, et all Gaussian, Inc., Wallingford CT, 2009.

[39] Becke AD. Density-functional thermochemistry. III. The role of exact exchange. J Chem Phys 1993; 98: 5648-5652. (b) Lee C, Yang W, Parr RG. Development of the Colle-Salvetti correlation-energy formula into a functional of the electron density. Phys Rev B 1988; 37: 785-789.

[40] Grimme S, Antony J, Ehrlich S, Krieg H. A consistent and accurate ab initio parametrization of density functional dispersion correction (DFT-D) for the 94 elements H-Pu. J Chem Phys 2010; 132: 154104-19.

[41] Boys SF, Bernardi F. The calculation of small molecular interaction by the differences of separate total energies. Mol Phys 1970; 19: 553-556.

[42] AIMAll (version 16.10.09), Todd AK, TK Gristmill Software, Overland Park KS, USA, 2016.

[43] Deeth RJ, Randell K. Ligand field stabilization and activation energies revisited: Molecular modeling of the thermodynamic and kinetic properties of divalent, first-row aqua complexes. Inorg Chem 2008; 47: 7377-7388.

[44] a) Hawkes SJ. All Positive Ions Give Acid Solutions in Water. J Chem Educ 1996; 73: 516-517. b) Baes CF, Mesmer RE. Hydrolysis of cations. Krieger RE Publishing Company: Malabar, FL, 1976.

[45] Harding MM, Nowicki MW, Walkinshaw MD. Metals in protein structures: A review of their principal features. Cryst Rev 2010; 16: 247–302.

[46] González-Moa MJ, Mandado M, Mosquera RA. Explaining the sequence of protonation affinities of cytosine with QTAIM. Chem Phys Lett 2006; 428: 255-261.

[47] Ferro-Costas D, Mosquera RA. Influence of the O-Protonation in the O═C–O-Me Z-Preference. A QTAIM Study. J Phys Chem A 2013; 117:257-265.

TOC Graphic